10.21611/qirt.2023.05

The Segmentation of Wind Turbine Defect Based on UAV Infrared Image

by Zijun Wang*, Naicheng Jiang,Ruizhe Wen and Bin Sun

* School of Aeronautics and Astronautics, University of Electronic and Technology of China, Chengdu 611731, China, *wangzijun@uestc.edu.cn*

Abstract

During the operation of wind power systems, problems such as damage may occur, in order to keep the system running normally and safely, regular maintenance of wind turbines is essential. Currently, the main treatment is to detect the blades by carrying an infrared camera on board a UAV. However, infrared images can suffer from significant inhomogeneities due to the inconsistent response of the detector array of the infrared camera, the inconsistent spectral response of the infrared detector to environmental variations and incoming background radiation, and the combined effect of the camera's optical lens. The inhomogeneity of an image can greatly affect the accuracy of image segmentation. To solve this problem, In this paper, we propose a method for rapidly segmenting inhomogeneous images. Specifically, we introduce global and local information of the image into the energy term. We also introduce a detail map as the reference map for the edge stopping function, which improves the robustness of the image to the initial contour and improves the segmentation accuracy of inhomogeneous images while speeding up the segmentation. Correction of bias field is also realized simultaneously. The results demonstrate that our method achieves average accuracy of 96% in the task of performing segmentation of wind turbine defects with the shortest running time. Notably, our segmentation efficiency surpasses that of mainstream level-set techniques.

Keywords: defect detection, bias correct, image segment.

1. Introduction

Wind power has recently received widespread attention as the most rapidly developing clean energy source, and its power generation capacity has greatly improved [1]. However, wind turbine blades may encounter damage and other problems during the operation of wind power. To ensure safe operation, routine inspection and maintenance is very necessary, and since wind power usually has a relatively high height, the current inspection method is mainly to use drones carrying infrared cameras to inspect them. In addition, infrared images can prevent interference from dust or markers and avoid false alarms during the detection process. Infrared images have been widely used in the field of detection, but due to the imaging principle of infrared images, infrared images usually have problems such as low contrast, high noise, and fuzzy edges, and the images often also have uneven intensity during the acquisition process [2-6]. The inhomogeneity of image intensity can have a great impact on image segmentation, and Kass et al. proposed a widely used model for inhomogeneous density images, active contour model (ACM) [7]. Meanwhile, the field of medical image segmentation faces similar problem with inhomogeneous images, in order to solve this problem, the level set method (LSM) is mainly used to segment the target, [8-11].Li et al. proposed Distance Regularized Level Set Evolution model (DRLSE) [12], which facilitates the convergence of active contours by using length and region terms, and introduces distance regularzation terms to avoid periodic initialisation energy. Liu et al. [13] proposed two-level-set DRLSE model to segment two targets. Wali et al. [14] computationally solved the DRLSE model by employing the alternating direction method of multipliers (ADMM) and achieved the effect of speeding up the solution process and improving the segmentation accuracy. Cai et al. [15] proposed a novel model that adaptively adjusts the scale of the level-set model by estimating the inhomogeneity of the image grey level and combining it with image entropy, further enhancing segmentation accuracy. Weng et al. [16] proposed combining the retinex model with the level set model to simulate and calculate the bias field. In addition, there are many methods that combine global and local image information in stages [17][18]. Some researchers have also extended the level set approach to color image segmentation [19][20].

Since infrared images often have the problem of image inhomogeneity, and the grayscale level inhomogeneity of an image can have a great impact on image segmentation, image segmentation in the case of grayscale level inhomogeneity has often received attention. In order to reduce the effect of image inhomogeneity on segmentation, our paper proposes a new level-set method combining multiple descriptors without manually inputting the initial contour. Firstly, we obtain a coarse segmentation result based on variable thresholding of local statistics and use it as the initial contour of the level-set algorithm, and then improve the edge stopping function by combining it with a guided filter, which results in a better performance. The combination of global and local information in the energy term, and the introduction of image entropy, and the estimation of bias field, have improved the accuracy and convergence time of the segmentation results. The main contributions of this method are as follows:

1) Introducing the detail map of the image as a guide map for the edge stopping function enhances both segmentation speed and accuracy.

2) Combining the global and local information of the image in the energy term reduces the problem of sensitivity to the initial contour of the level set method.

3) Combining the local threshold segmentation method further increases the segmentation speed and accuracy.

2. Background

2.1 Coarsely segment

As infrared images generally face more severe intensity inhomogeneities, the image is coarsely segmented using local statistical methods based on the image.

The local standard deviation of an image can be a better representation of the structural and detail information of the image. It also shows the degree of intensity variation, and the standard deviation is increased in areas with larger gradients. The local standard deviation can be obtained by the following formula:

$$v(m,n) = \frac{1}{9}\sum_{i=n-1}^{n+1} \sum_{j=m-1}^{m+1} [x(i,j) - \bar{x}(m,n)]^2 \tag{1}$$

Of which

$$\bar{x}(m,n) = \frac{1}{9}\sum_{i=n-1}^{n+1} \sum_{j=m-1}^{m+1} x(i,j) \tag{2}$$

The variable threshold based on the local image is defined as

$$T = a * v(x,y) + b * \bar{x}(x,y) \tag{3}$$

$m, \sigma$are the means and standard deviations of the pixels in the neighbourhood, respectively.

Then, we can get g as the result of the segment.

$$\begin{cases} g(x,y) = 1,\ f(x,y) > a * v(x,y) AND\ f(x,y) > b * \bar{x}(x,y) \\ g(x,y) = 0, others \end{cases} \tag{4}$$

This results in a coarse segmentation of the infrared image and the result is used as the initial contour for the iterative process of the level set algorithm.

2.2 Guided Filter

The guided filter is a local linear transform filter with good edge retention properties.

Its output can be expressed as

$$q_i = \sum_j W_{ij}(I) p_j \tag{5}$$

$$W_{ij}(I) = \frac{1}{|\omega|^2}\sum_{k:(i,j)\in\omega_k} \left(1 + \frac{(I_i - \mu_k)(I_j - \mu_k)}{\sigma_k^2 + \epsilon}\right) \tag{6}$$

where I is the guidance image, p is the input and q is the output image.

ω is the number of pixels in region ω_k, μ_k is the mean intensity value in the region, σ_k^2 is the intensity variance in the region and ϵ is the regularisation parameter of the penalty term.

By means of guided filtering, a detailed layer of the image can be obtained:

$$I_d = p - q; \tag{7}$$

The detail layer provides a good response to the boundary information of the area to be segmented in the image.

2.3 related models

2.3.1 CV models

Chan and Vese proposed a model based on global information of the image[21], which reduce the affect of the noise and the blurry of the boundary during the process of segmentation. The energy function of the CV model is defined as:

$$\begin{aligned} E_\varepsilon^{CV}(c_1, c_2, \phi) = \quad & \lambda_1 \int_\Omega |I(\mathbf{x}) - c_1|^2 H_\varepsilon(\phi(\mathrm{x}))d\mathbf{x} \\ & + \lambda_2 \int_\Omega |I(\mathbf{x}) - c_2|^2 (1 - H_\varepsilon(\phi(\mathrm{x})))d\mathbf{x} \\ & + \mu \cdot \int_\Omega \delta_\varepsilon(\phi(\mathbf{x}))|\nabla\phi(\mathrm{x})|dx \end{aligned} \tag{8}$$

where c_i represents the average value inside and outside the image, and λ_i and μ are the constants. ϕ denoting the level set.$H_\varepsilon(x), \delta_\varepsilon(x)$ present Heaviside function and Dirac function, respectively.

The formula for updating the energy function can then be obtained by the gradient descent method.

$$\frac{\partial\phi}{\partial t} = \delta_\varepsilon(\phi)\left[-\lambda_1(I(\mathbf{x}) - c_1)^2 + \lambda_2(I(\mathbf{x}) - c_2)^2 + \mu div\left(\frac{\nabla\phi}{|\nabla\phi|}\right)\right] \tag{9}$$

However, the CV model evolves very slowly and does not work well enough for inhomogeneous image segmentation.

2.3.2 LBF model

The LBF model is based on local information and solves the problem of segmenting intensity inhomogeneous images by considering the intensity distribution to be uniform within a local region.[22] A Gaussian window function is used

to obtain the average internal and external grey values of the image in the local area of the evolution curve as energy. The energy function of the LBF model is defined as:

$$\begin{aligned} E^{LBF}(f_1, f_2, \phi) = \lambda_1 \int \left[\int K(\mathbf{x}-\mathbf{y})|I(\mathbf{y}) - f_1(\mathbf{x})|^2 H_\varepsilon(\phi(x))d\mathbf{y}\right]d\mathbf{x} \\ +\lambda_2 \int \left[\int K(\mathbf{x}-\mathbf{y})|I(\mathbf{y}) - f_2(\mathbf{x})|^2 d\mathbf{y}\right][1 - H_\varepsilon(\phi(x))]d\mathbf{x} \\ +\mu \cdot \int \frac{1}{2}(|\nabla\phi(\mathbf{x})| - 1)^2 d\mathbf{x} + \nu \cdot L(\phi(\mathbf{x})) \end{aligned} \tag{10}$$

The LBF model is relatively effective in segmenting inhomogeneous images because local information is considered, but the model is sensitive to the initial position of the contours because global information is not considered.

2.3.3 DRLSE model

Li et al. propose a method that does not require reinitialization of the level set. They use the boundary stop function to guide the curve to converge to the contour boundary. The energy function may be expressed as:

$$E(\phi) = \lambda \int g(x)\delta(\phi)|\nabla\phi|dx + \nu \int g(x)H(-\phi)dx + \mu \int R(|\nabla\phi|)dx \tag{11}$$

The three terms in the energy function are the edge detection term, the area term, and the penalty term.

of which

$$R(|\nabla\phi|) = \begin{cases} \frac{1}{(2\pi)^2}[1 - \cos(2\pi|\nabla\phi|)], & |\nabla\phi| < 1, \\ \frac{1}{2}(|\nabla\phi| - 1)^2, & |\nabla\phi| \geq 1. \end{cases} \tag{12}$$

It is possible to make the level set function 1 near the zero level set and the gradient modulus 0 away.

The edge indicator g(x) is defined as

$$g(x) = \frac{1}{1 + \left|\nabla G_\sigma * I(x)\right|^2} \tag{13}$$

However, the DRLSE algorithm is very sensitive to the initial contour of the segmentation and will have different segmentation results for different initial contours, so it is not very suitable in some cases.

Samad et al. compute DRLSE model by using the ADMM algorithm. This algorithm is significantly more effective in identifying the boundaries of regions of interest and reduces the time taken by the algorithm.

2.3.4 ABC model

Weng proposed additive bias correction (ABC) model based on intensity inhomogeneity. They integrate RETINEX model into level set model to get a ideal segmentation for intensity inhomogeneity images.

They define the observed image as:

$$i(\boldsymbol{x}) \approx b_j(\boldsymbol{x}) + r(\boldsymbol{x}) + n(\boldsymbol{x}) \text{ for } \boldsymbol{x} \in \Omega_j \tag{14}$$

So, they rewrite the energy function as

$$E^{ABC}(\varphi, r, \boldsymbol{b}) = \int \sum_{i=1}^{2} \left(\int G_\sigma(\boldsymbol{y}-\boldsymbol{x})\left|i(\boldsymbol{x}) - r(\boldsymbol{y}) - b_j(\boldsymbol{y})\right|^2 d\boldsymbol{y}\right) M_j(\varphi(\boldsymbol{x}))d\boldsymbol{x} \tag{15}$$

In addition, the method introduces the activation function tanh to enhance the accuracy of the bounds, rewrites equation (15) and reduces the length and regularization terms in the level set algorithm, reducing the complexity of the algorithm.

$$\frac{\partial\varphi}{\partial t} = -\alpha\delta(\varphi)\tanh\left(\frac{(e_1 - e_2)}{\beta}\right) \tag{16}$$

$$\beta = \sqrt{\frac{1}{M \times N}\sum_{i=1}^{M}\sum_{j=1}^{N}(I(i,j) - \bar{I}(i,j))^2} \tag{17}$$

$$e_j(\boldsymbol{x}) = \int G_\sigma(\boldsymbol{y}-\boldsymbol{x})\left|i(\boldsymbol{x}) - r(\boldsymbol{y}) - b_j(\boldsymbol{y})\right|^2 d\boldsymbol{y} \tag{18}$$

β is the standard deviation of the image.

3. Proposed model

In this paper, a multiplicative model is used to represent the observed images to address the intensity inhomogeneity of the images:

$$I = bJ + n \tag{19}$$

Where I is the observed image, b is the bias field on the image, J is the ideal image of uniform intensity and n is the noise. Where, for the bias field b, it is assumed that it varies slowly in the spatial domain and that each point can be approximated by a neighbourhood representation. For the ideal image J, the N disjoint regions can be approximated by N independent constants expressing N disjoint regions. By combining this model with the level set function energy formulation, this enables the possess of image segmentation and bias estimation could be done at the same time. To address the sensitivity of the level set method to the initial contours, two methods are proposed to enhance the robustness of the model to the initial contours.

1. coarse segmentation of the input defect image by local standard deviation to ensure that errors in the position of the initial contour and the actual contour do not cause mis-segmentation or edge leakage.

2. initialise the bias, in the process of introducing the bias field for iteration, most models such as the LIC(local intensity cluster) model define the initial bias as a matrix with element 1, at which point the initial state of the model

degenerates into a CV model, and the cv model does not perform well in segmenting inhomogeneous images, with weak boundary images, and may lead to errors in image segmentation.

In this paper, the energy generalisation of the level set function is defined as follows.

$$E(\phi,b,c)=\varepsilon^{A}+\varepsilon^{B}+\varepsilon^{c} \tag{20}$$

where ε^{A}, ε^{B} and ε^{C} denote the data term, the area term, and the penalty term, respectively, and they can be written as:

$$\begin{cases} \varepsilon^{A}=\lambda_1\int_{\Omega}h_x K_\sigma *(f(x)-bc_1)^2 H(\varphi(x))dx-\lambda_2\int_{\Omega}h_x K_\sigma *(f(x)-bc_2)^2(1-H(\varphi(x)))dx \\ \varepsilon^{B}=\mu\int_{\Omega}g(f(x))H(-\varphi(x))dx \\ \varepsilon^{C}=\alpha\int_{\Omega}p(|\nabla\varphi(x)|)dx \end{cases} \tag{21}$$

c_1, c_2 represents the average intensity of the inner and outer contours, respectively, calculated as

$$\mathrm{c}_i=\frac{\int_{\Omega}f(x)M_i(\phi(x))dx}{\int_{\Omega}M_i(\phi(x))dx},\quad M_1(\phi(x))=H(\phi(x)),M_2(\phi(x))=1-H(\phi(x)) \tag{22}$$

By introducing global variables, the influence of the initial profile before the iteration on the evolutionary results can be reduced and robustness increased.

For the data term ε^{A} which acts to split the image into two homogeneous regions, the function $K_\sigma(x)$ is a Gauss function with variance σ. The local intensity information of the image can be obtained by convolving the Gauss function. Combined with the local Shannon entropy of the image, the local Shannon entropy is introduced into the energy general function model, which can reflect the intensity variation characteristics within the neighbourhood of the image and ensure the processing of intensity inhomogeneous images. To improve the accuracy and enhance the noise immunity, the local entropy of the image is introduced, which has the property of reflecting the intensity change within the reaction area. The expression of local entropy is given by.

$$h_x(p(y))=-\int_0^L p_x(y)\log_2 p_x(y)dy \tag{23}$$

Where h_x is the local entropy of pixel x, $p_x(y)=n_y/(m\times n)$ is the probability density estimate of the grey level y in the $m\times n$ neighbourhood, and n_y is the number of pixels with grey level y in the $m\times n$ neighbourhood.

$$g(f(x))=\frac{1}{1+\exp(\rho\bullet I_d)\left|\nabla G_\sigma * f(x)\right|^2} \tag{24}$$

ρ is the normalisation factor and is the image detail layer obtained through the guided filtering, which can reflect the image edge information well and is favourable to the stop function for edge preservation. The introduction of a detail layer helps to improve segmentation accuracy and speed up segmentation. In the smooth region of the image, I_d tend to 0, while $\left|\nabla G_\sigma * f(x)\right|$ being smaller, makes g(f(x)) converge to 1. Similarly, g(f(x)) converges to 0 in the border part of the image.

The penalty term is ε^{C}. The level set function often oscillates periodically during curve evolution and must be periodically reinitialised as a signed distance function. to avoid reinitialisation, a penalty term is used to avoid complex reinitialisation. Cai Qing proposes a new penalty term to improve the neglect of energy minima and thus increase the accuracy of the algorithm segmentation.

$$\begin{aligned} p(s)&=\begin{cases}\frac{1}{5}s^3-\frac{3}{10}s^2+\frac{1}{10}, & s\le 1\\ \frac{1}{2}(s-1)^2, & s>1\end{cases}\\ p'(s)&=\begin{cases}\frac{3}{5}s(s-1), & s\le 1\\ s-1, & s>1\end{cases}\\ d_p(s)&=\begin{cases}\frac{3}{5}(s-1), & s\le 1\\ 1-\frac{1}{s}, & s>1\end{cases}\end{aligned} \tag{25}$$

Because it is more difficult to calculate the $H(x)$ function in practice, the smooth continuous *Heaviside* and *Dirac* functions are often used:

$$H_\varepsilon(s)=\frac{1}{2}(1+\frac{2}{\pi}\arctan\frac{s}{\varepsilon}) \tag{26}$$

The approximate *Dirac* function is obtained by deriving H_ε(s) as follows:

$$\delta_\varepsilon = \frac{\varepsilon}{\pi(\varepsilon^2 + s^2)} \tag{27}$$

The complete energy function can be expressed as

$$\begin{aligned} E(\phi,b,c) = {} & \lambda_1 \int_\Omega h_x K_\sigma * (f(x) - bc_1)^2 H(\phi(x))dx \\ & - \lambda_2 \int_\Omega h_x K_\sigma * (f(x) - bc_2)^2 (1 - H(\phi(x)))dx \\ & + \mu \int_\Omega g(f(x)) H(-\phi(x))dx + \alpha \int_\Omega p(|\nabla\phi(x)|)dx \end{aligned} \tag{28}$$

By holding ϕ in the energy function fixed, a minimisation of b results in

$$b = \frac{(IJ_1) * K}{J_2 * K}; J_1 = c_1 H(\phi) + c_2(1 - H(\phi)), J_2 = {c_1}^2 H(\phi) + {c_2}^2 (1 - H(\phi)) \tag{29}$$

Solved by variational theory and gradient descent flow method to obtain.

$$\frac{\partial\phi}{\partial t} = -\delta_\varepsilon(\phi)\left(\lambda_1 e_1 - \lambda_2 e_2\right) + \mu g(f(x))\delta_\varepsilon(\phi) + \alpha \mathrm{div}(d_p(|\nabla\phi|)\nabla\phi) \tag{30}$$

Which $e_i = h_x K_\sigma (f(x) - bc_i)^2$

An explicit finite difference strategy is used to discretize Eq(30).

$$\frac{\phi^n - \phi^{n-1}}{\Delta t} = -\delta_\varepsilon(\phi)\left(\lambda_1 e_1 - \lambda_2 e_2\right) + \mu g(f(x))\delta_\varepsilon(\phi) + \alpha \mathrm{div}(d_p(|\nabla\phi|)\nabla\phi) \tag{31}$$

The initial energy function of the level set can be obtained by the formula.

$$\phi_0 = (0.5 - g) * 2 * c_0 \tag{32}$$

As damage usually has a small area, the level set function is further binarized to reduce the effect of mis-segmentation.

$$\begin{cases} BW = 1, if\ \phi < 0 \\ BW = 0, if\ \phi \geq 0 \end{cases} \tag{33}$$

Suppose there are n independent regions with BW value 1 as $\Omega_1, \Omega_2 \cdots \Omega_n$respectively, define $N_i$as the number of pixels in the ith region, if $N_i > \eta$,then $BW(x) = 0, x \in \Omega_i$. where η is a chosen threshold value.

Recalculation c_1, c_2.

$$\mathrm{c}_i = \frac{\int_\Omega f(x) M_i(x)dx}{\int_\Omega M_i(x)dx}, \quad M_1(\phi(x)) = BW(x), M_2(\phi(x)) = 1 - BW(x) \tag{34}$$

and update to obtain the bias field b.

$$b = \frac{(IJ_1) * K}{J_2 * K}; J_1 = c_1 BW(x) + c_2(1 - BW(x)), J_2 = {c_1}^2 BW(x) + {c_2}^2 (1 - BW(x)) \tag{35}$$

Because of $I = bJ + n$. Assuming that the noise is removed after processing. We can get the ideal image J by

$$J = \frac{I}{b} \tag{36}$$

The algorithm flow proposed in this paper is as follows:

1 The initial contour of the segmentation is obtained by variable threshold processing based on local statistics, and the level set function is initialized according to the contour. It can be calculated by Eq. (32).
2 Obtain the detail layer I_d according to Eq. (7)
3 For $k = 1{:}n$;
(1) Compute $c_1, c_2$by Eq. (22).
(2) Obtain the estimated bias field b according to Eq. (29).
(3) Evolve the level set function according to Eq. (31).
4 Obtain the image binary mask according to the level set function to confirm the segmentation region.
5 Calculate BW from Eq. (33)
6 Recalculate c_1, c_2 and update the bias field according to Eq. (34,35)
7 Output the Image after correction of bias field from Eq. (36).

The time required by this algorithm to perform the segmentation is 6s and 18s respectively. The result of the segment and the image after bias correction are shown in Fig.1

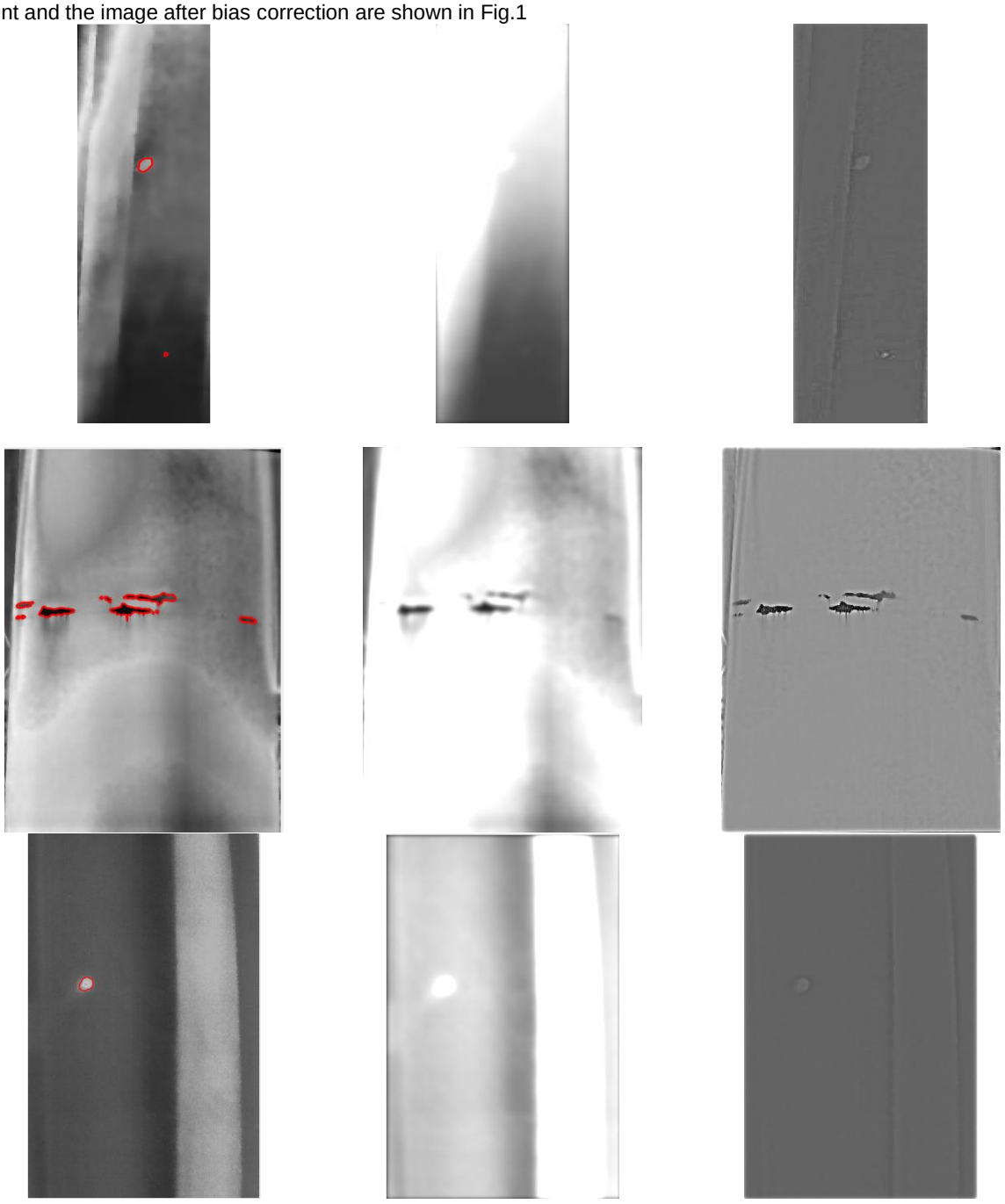

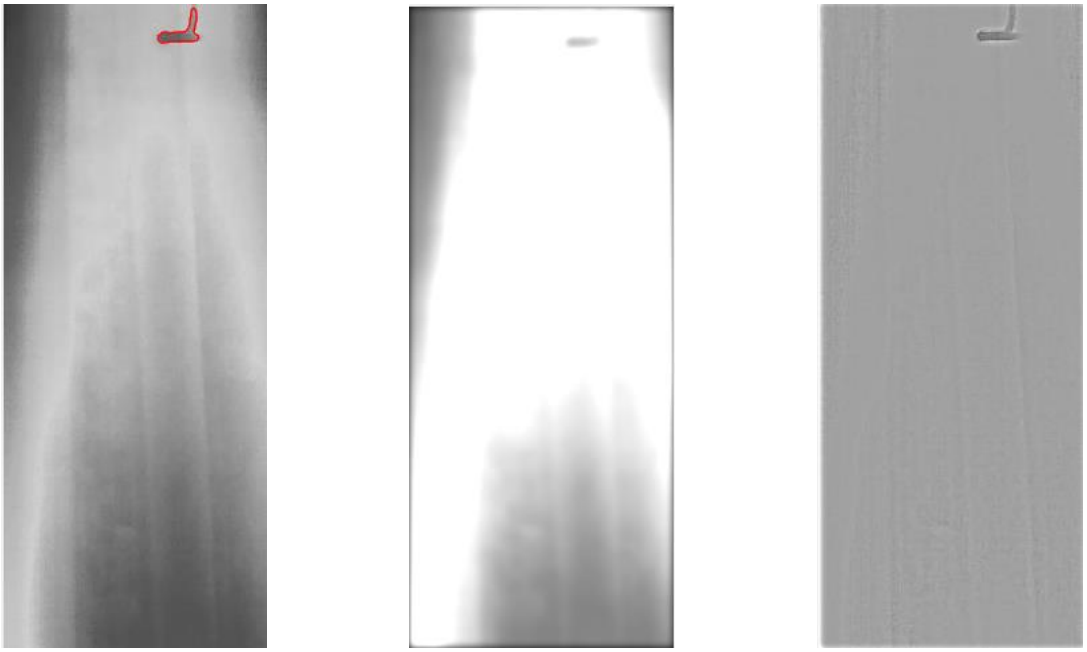

Segment result Bias field bias correction

Fig. 1. *The result of segment and correction*

4. Experimental result

In this section, we will use the method of obtaining infrared images of the defective part in the field with a UAV equipped with an infrared camera, all the experiments will be run on MATLAB through a PC with intel i7 2.3GHz CPU and 16GB RAM. In addition, the parameters in the experiments are set as follows:

$c_0 = 2, \lambda_1 = \lambda_2 = 1, \sigma = 3.0, \mu = 0.002*255*255, \alpha=1, \eta=900, \Delta t=0.15;$

In order to compare the effectiveness of each method for the segmentation effect, the defective places of the target image will be labelled by manual labelling method, and two values below will be used in this paper to judge the segmentation accuracy as well as the edge leakage. Ground truth is shown in Fig. 2.

$$Accuracy = \frac{\Omega_{x \in Groundtruth} \cap \Omega_{x \in segmentresult}}{\Omega_{x \in Groundtruth}} \tag{37}$$

$$Leakage = \frac{\Omega_{x \notin Groundtruth} \cap \Omega_{x \in segmentresult}}{\Omega_{x \subseteq segmentresult}} \tag{38}$$

It can be seen that along with higher $Accuracy$, it proves that the segmentation of the image is able to contain the defective part effectively, and smaller leakage represents smaller mis-segmented region, so when accuracy is higher along with smaller $Leakage$ can indicate that the image segmentation is more accurate.

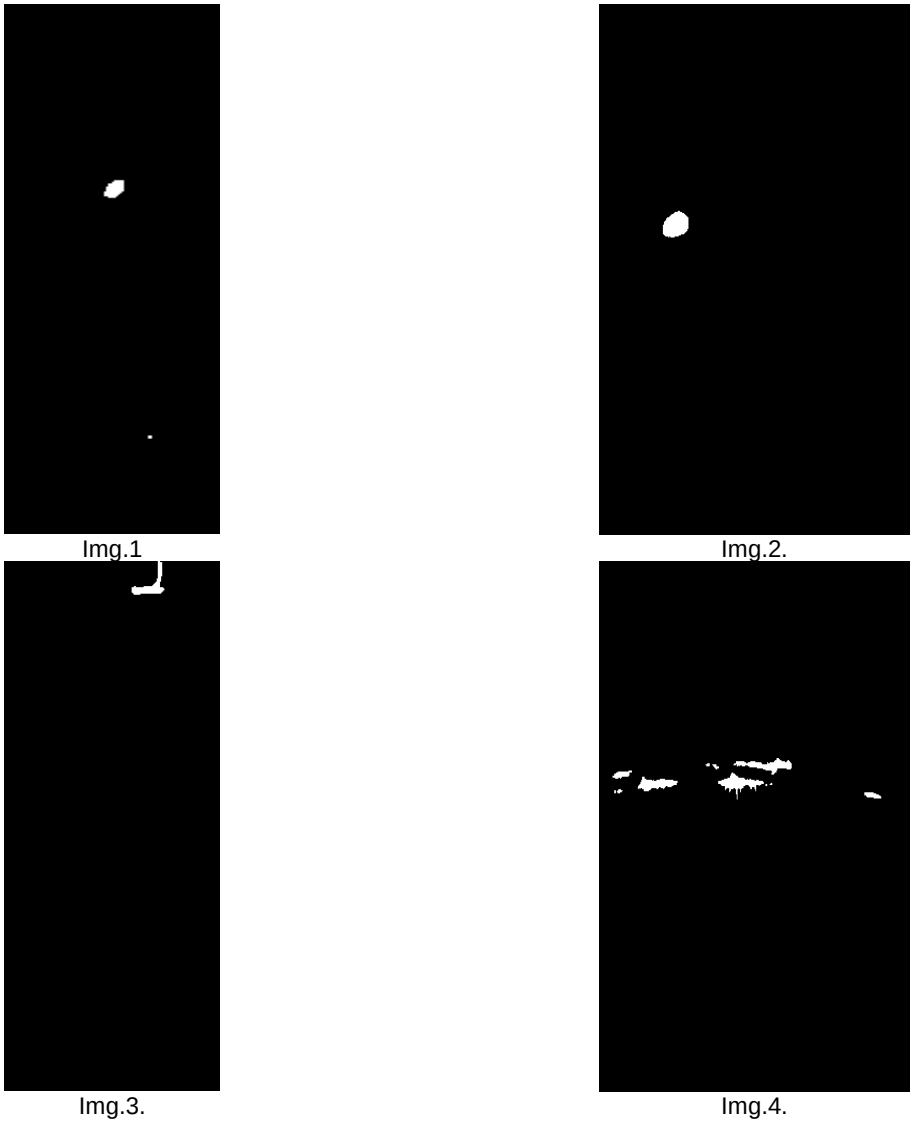

Img.1 Img.2.

Img.3. Img.4.

Fig. 2. *The Ground truth of segment to Images*

Table 1*. Metrics of each method for different images (bolded values for best results for graphs)*

Accuracy/Leakage	proposed	cv	ABC	DRLSE	ADMM-DRLSE	LBF
Img.1	0.9651 /**0.0778**	0.3488 /0.9971	0.9419 /0.9812	0.8256 /0.3932	0/1	**0.9884** /0.9968
Img.2	**0.9917** /0.012	0.4254 /0.9908	0.5395 /0.9841	0.6689 /**0**	0.4123 /0.9940	0.4605 /0.9851
Img.3	0.9192 /**0.0808**	0.91 /0.9959	**0.9239** /0.8166	0.6886 /0.1459	0.4637 /0.9980	0.7647 /0.8383
Img.4	0.9667 /**0.1063**	0.9641 /0.8661	0.8772 /0.8764	0.8922 /0.6878	**0.9765** /0.9833	0.9667 /0.9222

4.1 Algorithm efficiency analysis

To test the effect of bias field correction. At the same time, to better illustrate the effectiveness of the present model, this was compared with DRLSE, LBF, ABC, ADMM-DRLSE and CV model, the model parameters are set with reference to the respective literature, as the images are actually taken, a subjective approach is used to determine the segmentation accuracy, as well as the program running time is used to obtain the efficiency of the algorithm. The efficiency of the algorithm in this paper can be proved directly through Fig.3. As shown in Fig.4 to Fig.7, the method proposed in this paper can accurately find the real boundary and can segment the target boundary in a relatively short time, and has the characteristics of not affected by the initial contour, the segmentation speed is fast.

In order to compare the segmentation effect of each algorithm on the damage region under different conditions, the damage in four different cases are compared here. In the case of image 1 (Fig.4), the infrared image has a relatively small resolution with strong inhomogeneity, and in the face of the small target segmentation of Img. 1, the method proposed in this paper can segment it better, and it can be seen by comparing it with the manually labelled image that the segmented four-pixel points are consistent with the actual region to be segmented. By comparing the proposed evaluation metrics, the proposed method can greatly reduce the mis-segmentation under normal regions while including the majority of defective region pixels.

In order to compare the boundary segmentation ability of the algorithm for weak boundary targets, Img. 2 (Fig.5) obtained during the shooting process will be used to compare the segmentation effect. The algorithm in this paper is able to segment regions with fuzzy boundaries with significantly better accuracy than the other algorithms and maintains very little leakage.

The infrared image where the target is at the edge of the image like Img.3 (Fig.6) is selected as the experimental object for processing, and it can be found that the algorithm proposed in this paper can accurately segment the target under the condition of ensuring that there will be no mis-segmentation.

Finally, as the level set algorithm in the face of the more dense non-connected targets easily caused by the segmentation results of different targets connected, so Img. 4 (Fig.7) used the visible image and infrared image alignment fusion processing operation, the figure contains a large number of damage region, which also contains a certain number of small targets, and the pixel distance is very close to the pixel distance, by comparing the various algorithms, it can be obviously seen that this paper's algorithm by comparing the algorithms, it is obvious that the algorithm in this paper can accurately segment each region independently. The advantages of the algorithm proposed in this paper can be compared more clearly through Fig.8.

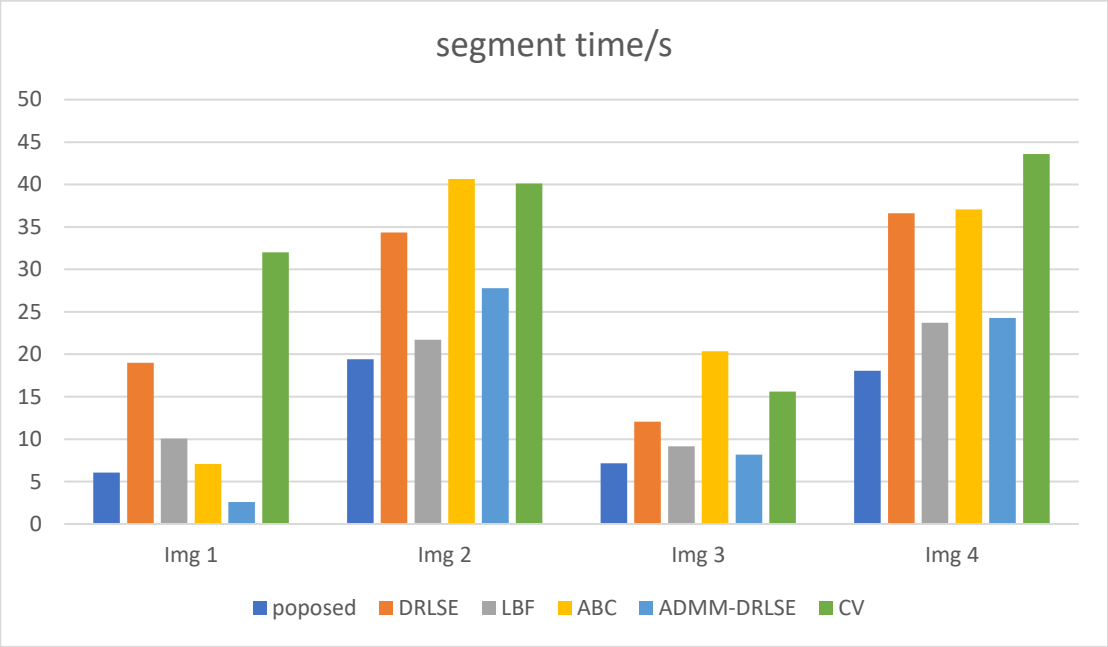

Fig. 3. *Time required for different algorithms to segment different images respectively*

4.2 Analysis of bias field estimation

Fig.9. can clearly see the effect of bias field estimation, the intensity image of the bias field can be obtained in the algorithmic process, and the image after bias field correction is shown, it can be clearly observed that the intensity non-uniformity of the corrected image is optimized, which has a significant improvement in the segmentation accuracy. Comparing the ABC algorithm, it can be seen that the proposed algorithm in this paper has improved the inhomogeneity correction of the image. Also, this action increases the accuracy of image segmentation under inhomogeneous conditions. In order to show more intuitively how well the algorithm corrects for image inhomogeneity, Nonuniformity is used to evaluate the algorithm's residual of nonuniformity. The value of Nonuniformity is obtained by calculating through equation (39).

$$NU = \frac{1}{\bar{Y}}\sqrt{\frac{1}{MN}\sum_i^M \sum_j^N \left(Y_{ij} - \bar{Y}\right)^2} \tag{39}$$

Where Y_{ij} is the gray value of point (i,j) of the image $\bar{Y}$ is the mean gray value of the image and M,N is the length and width of the image respectively. The algorithm proposed in this paper and the ABC algorithm to get the bias field corrected images to determine the residual image inhomogeneity by the NU value, the NU value of the corrected maps of the two algorithms for the four images are recorded in Table 2. After comparison it can be found that the algorithm proposed in this paper also has better results in the effect of non-uniformity correction.

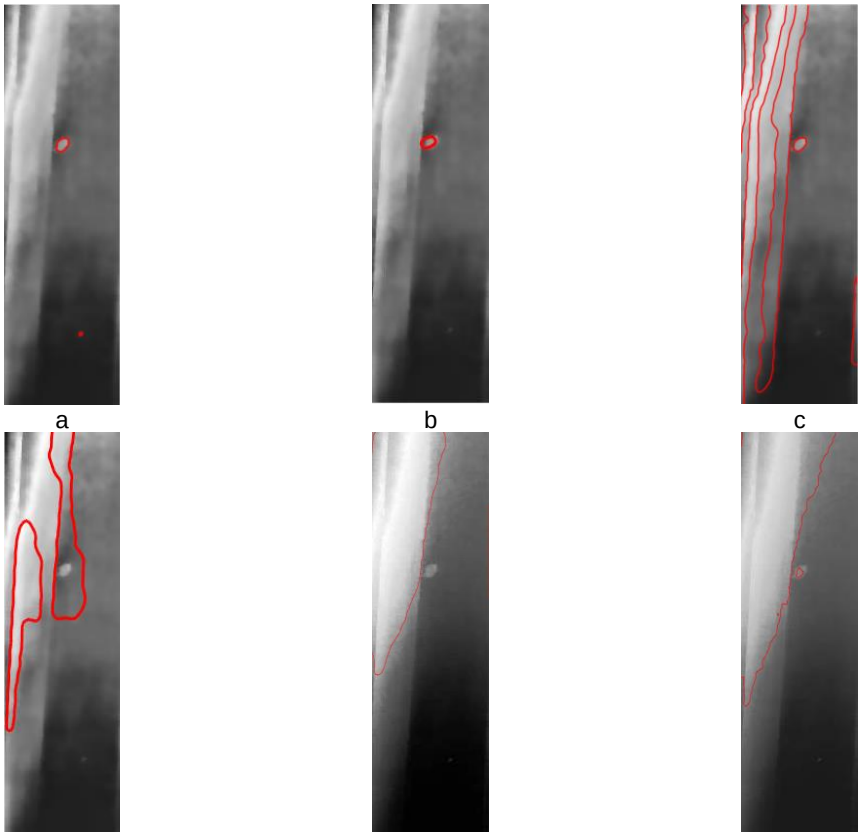

Fig.4. *the segmentation of image 1. a) is the proposed method, t=6.06s; b) DRLSE t=18.98s c) LBF t=10.06s d) ABC t=7.06s e) ADMM-DRLSE t=2.6s f) CV t=32s*

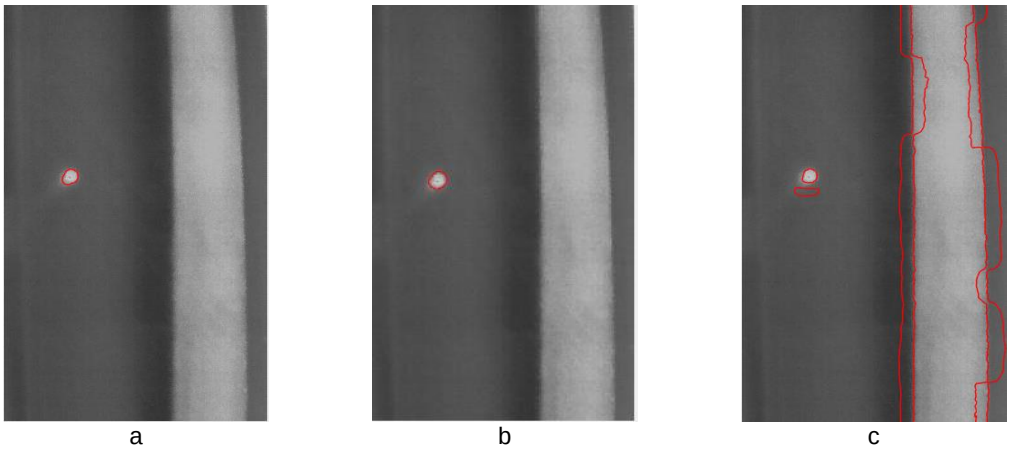

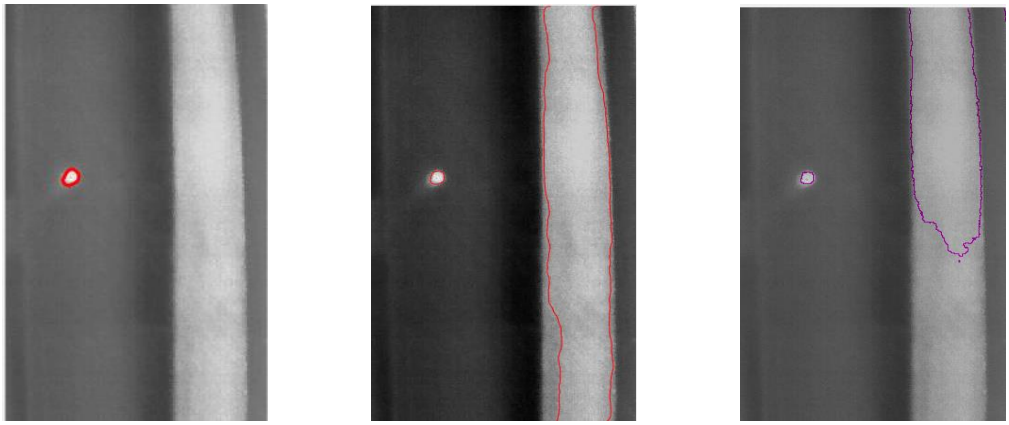

d e f

Fig.5 *the segmentation of image 2. a) is the proposed method, t=19.42s; b) DRLSE t=34.35s c) LBF t=21.7s d) ABC t=40.65s e) ADMM-DRLSE t=27.77s f) CV t=40.12s*

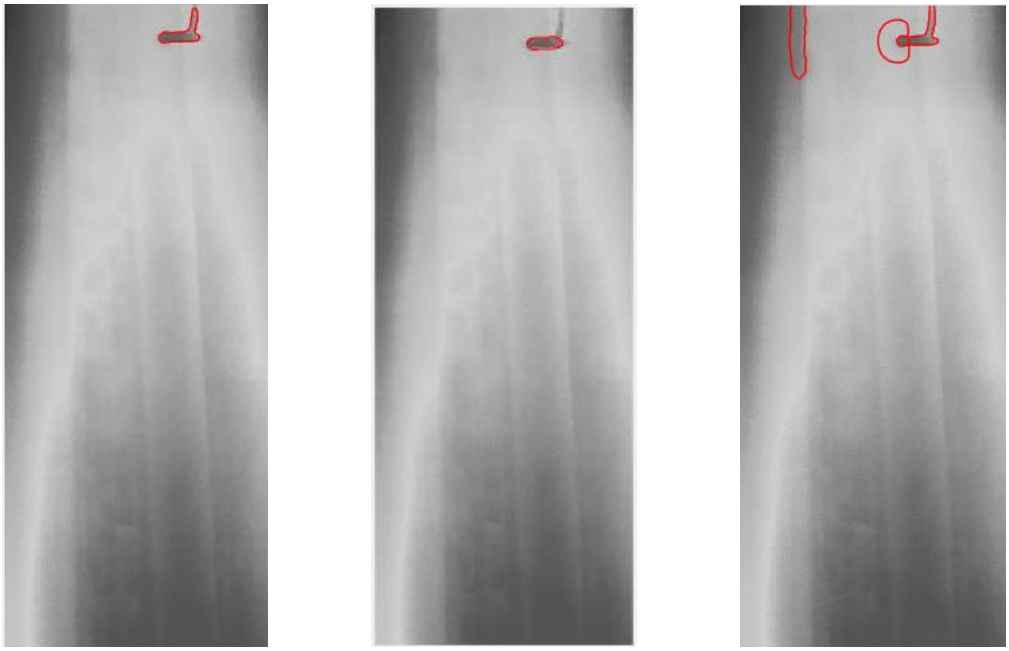

a b c

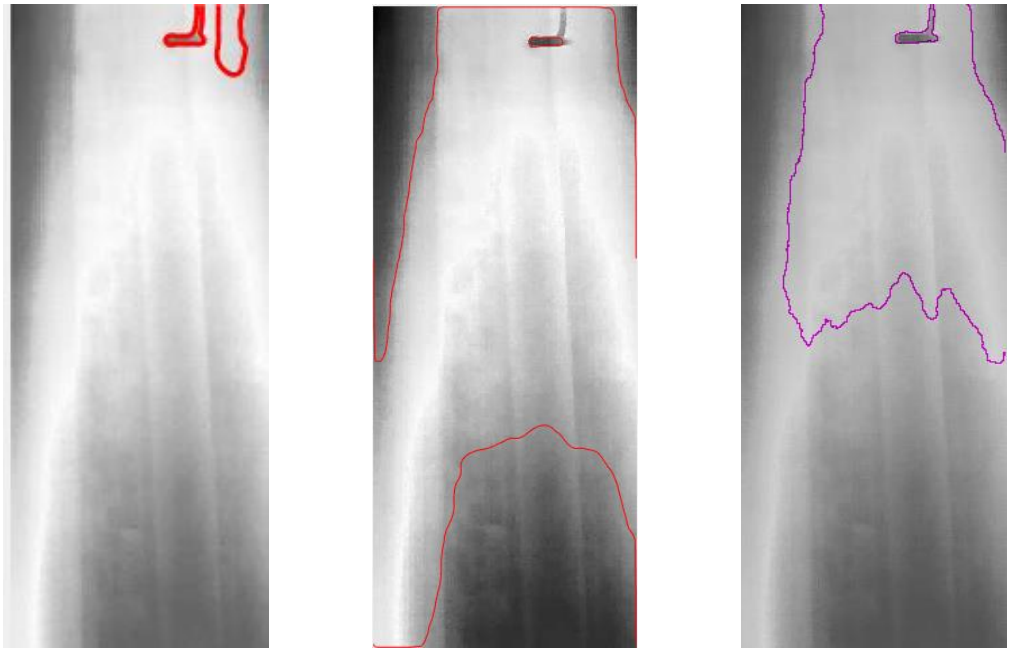

d e f

Fig.6 *the segmentation of image 3. a) is the proposed method, t=7.15s; b) DRLSE t=12.04s c) LBF t=9.17s d) ABC t=20.37s e) ADMM-DRLSE t=8.16s f) CV t=15.6s*

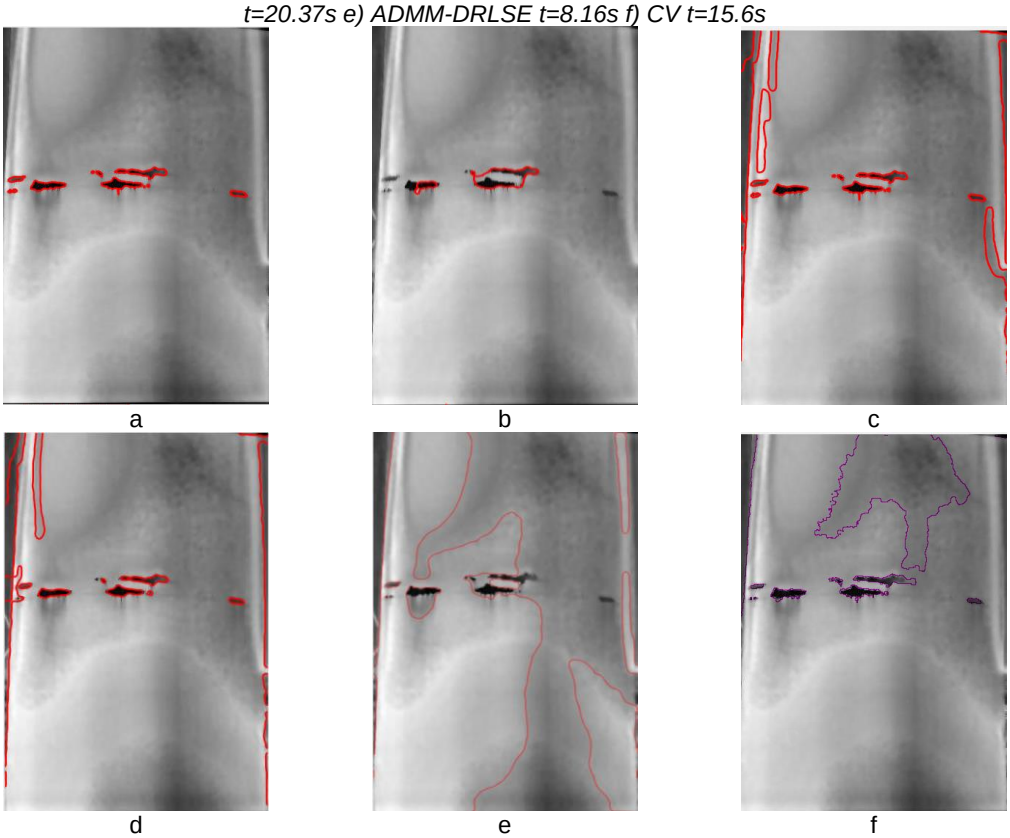

a b c

d e f

Fig.7 *the segmentation of image 4. a) is the proposed method, t=18.04s; b) DRLSE t=36.6s c) LBF t=23.7s d) ABC t=37.06s e) ADMM-DRLSE t=24.26s f) CV t=43.6s*

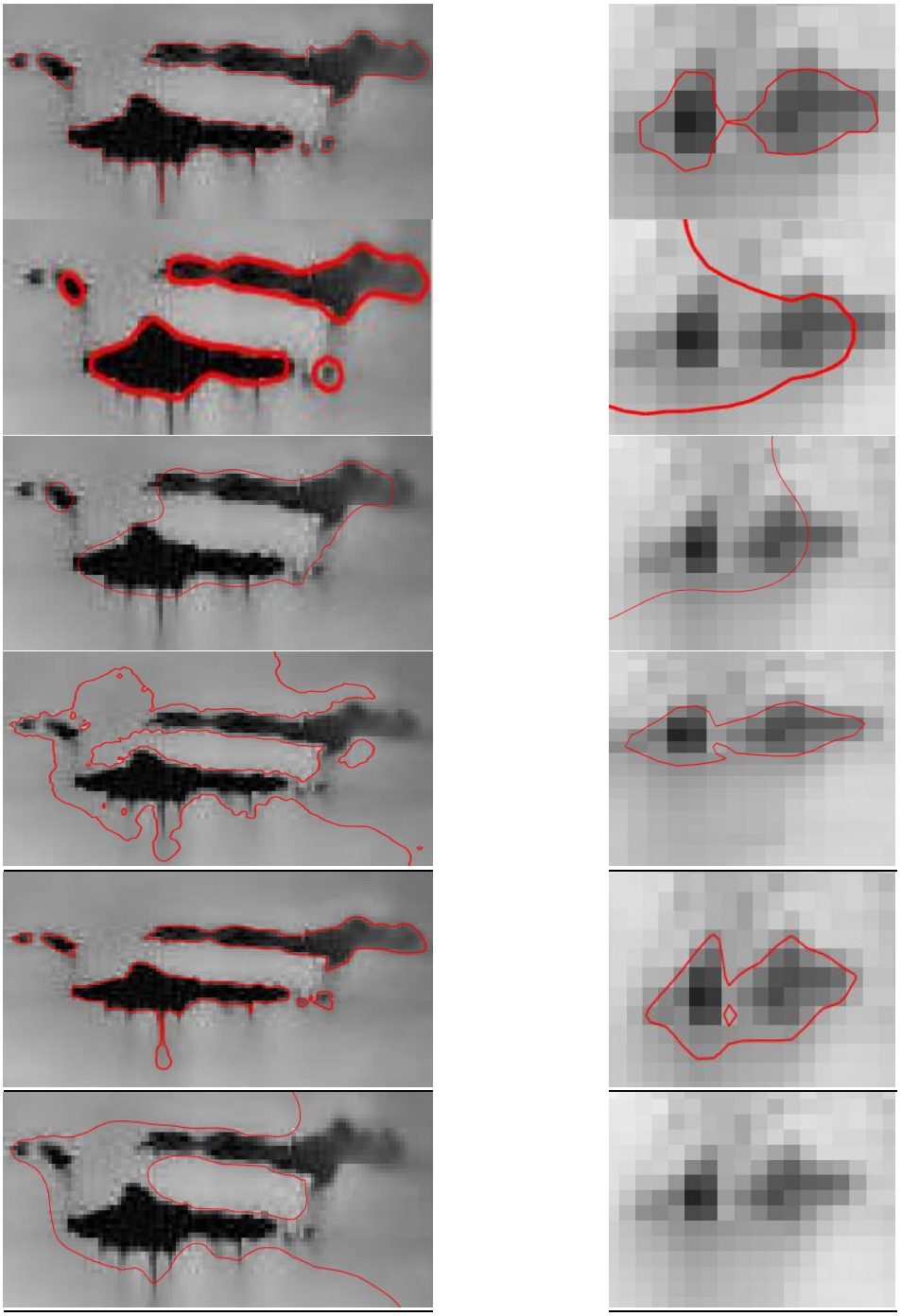

Fig.8 *Img.3 the detailed comparison of segmentation results. The proposed algorithm, ABC, DRLSE, CV, LBF and ADMM-DRLSE algorithms are used in each column respectively.*

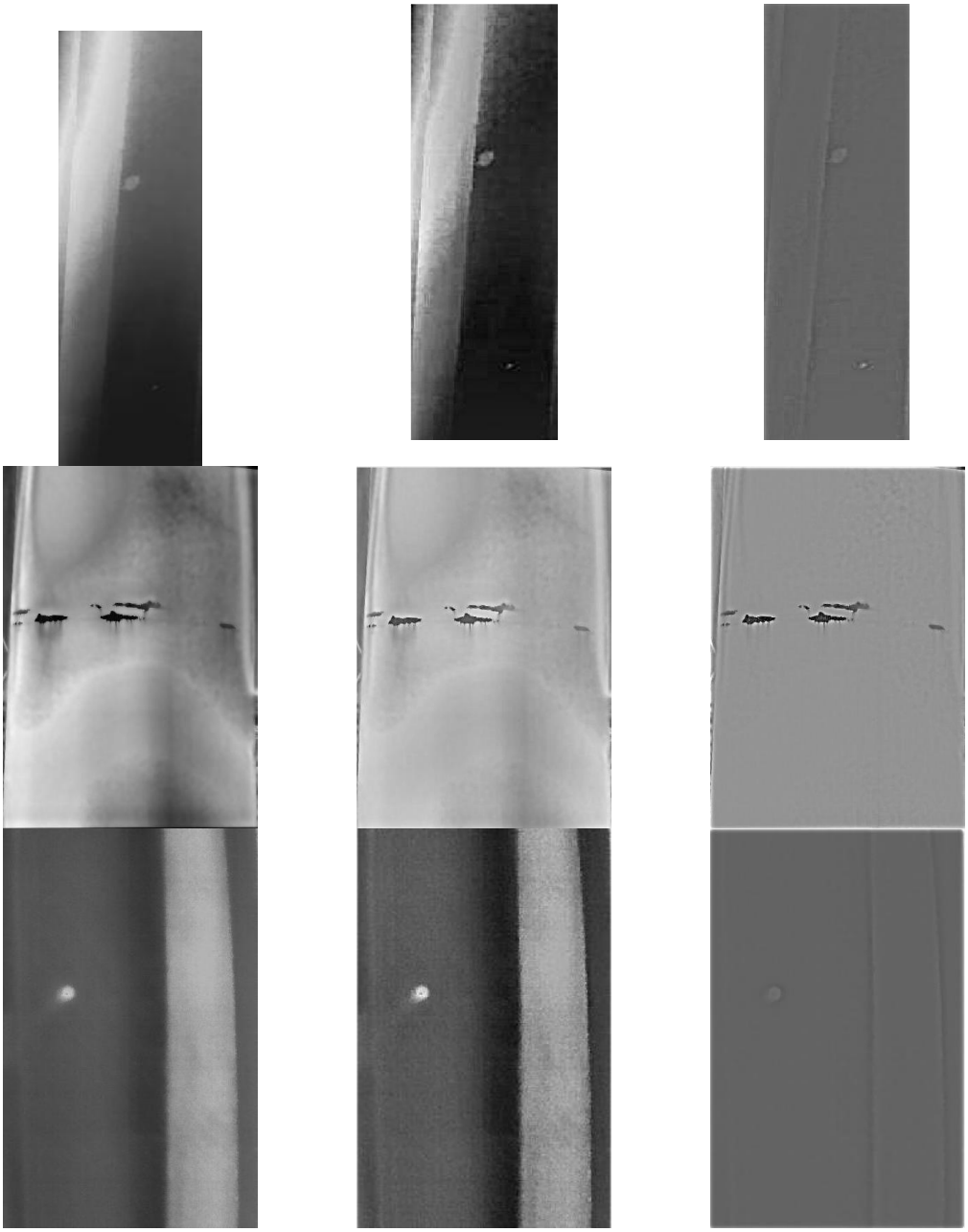

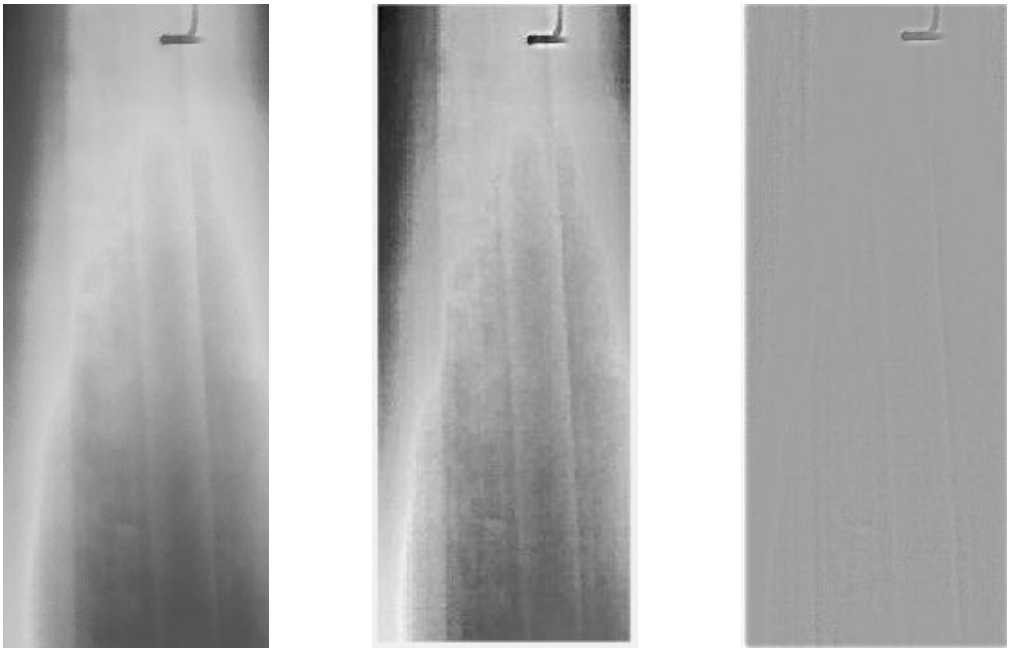

a b c

Fig.9 *a) is the original image; b) is the result of ABC algorithm to correct for image inhomogeneity c) is the result of proposed method to correct for image inhomogeneity*

***Table 2**. NU values of images corrected by proposed algorithm and the ABC algorithm*

	Img1	Img2	Img3	Img4
Proposed	0.1416	0.0960	0.0895	0.1074
ABC	0.5516	0.3937	0.2173	0.1056

5. Conclusion

In order to ensure the normal operation of wind turbines, regular testing and maintenance are very necessary. Drones equipped with infrared cameras are used to shoot the wind power equipment, and infrared images can effectively avoid the influence of dirt on damage area assessment. After shooting the equipment with damage, the damage area is a very necessary measure, but due to the infrared camera imaging principle and equipment limitations, infrared images often have the problem of uneven intensity. This problem will seriously affect the segmentation of defects. In this regard, an active contour model based on multiple descriptors and combining local and global information can effectively segment the intensity inhomogeneous image accurately and correct its inhomogeneity. Our method can effectively avoid the sensitivity of the level set method to the initial contour, while realizing the automatic segmentation of defects. After a number of experiments to verify, our algorithm can carry out accurate segmentation in a relatively short period of time, and can largely suppress the inhomogeneity of the image, and can also achieve good segmentation results for targets with weak boundaries.

6. Acknowledgements

ZW would like to thank the financial support provided by the National Natural Science Foundation of China (Grant No. 61905038) and Natural Science Foundation of SiChuan (Grant No. 2022NSFSC0967).

REFERENCES

[1] Chen, Zhe, Josep M. Guerrero, and Frede Blaabjerg. ‘A Review of the State of the Art of Power Electronics for Wind Turbines’. IEEE Transactions on Power Electronics 24, no. 8 (August 2009): 1859–75. https://doi.org/10.1109/TPEL.2009.2017082.

[2] Wang, Yi, Zhonghua Luo, Zhihai Xu, Huajun Feng, Qi Li, and Yueting Chen. ‘Fusion of Infrared and Visual Images through Multiscale Hybrid Unidirectional Total Variation’. In 2016 IEEE International Conference on Signal and Image Processing (ICSIP), 41–46, 2016. https://doi.org/10.1109/SIPROCESS.2016.7888220.

[3] Voronin, Vyacheslav, Evgenii Semenishchev, Oxana Balabaeva, and Marina Pismenskova. 'Preprocessing Images And Restore The Contours Of Objects Obtained In The Infrared Range'. In 2018 14th IEEE International Conference on Signal Processing (ICSP), 430–33, 2018. https://doi.org/10.1109/ICSP.2018.8652422.
[4] Voronin, Viacheslav, Svetlana Tokareva, Evgenii Semenishchev, and Sos Agaian. 'Thermal Image Enhancement Algorithm Using Local And Global Logarithmic Transform Histogram Matching With Spatial Equalization'. In 2018 IEEE Southwest Symposium on Image Analysis and Interpretation (SSIAI), 5–8, 2018. https://doi.org/10.1109/SSIAI.2018.8470344.
[5] Fan, Fan, Yong Ma, Jun Huang, and Zhe Liu. 'Infrared Image Enhancement Based on Saliency Weight with Adaptive Threshold'. In 2018 IEEE 3rd International Conference on Signal and Image Processing (ICSIP), 225–30, 2018. https://doi.org/10.1109/SIPROCESS.2018.8600468.
[6] Chen, Yunjie, Jianwei Zhang, and Jianwei Yang. 'An Anisotropic Images Segmentation and Bias Correction Method'. Magnetic Resonance Imaging 30, no. 1 (January 2012): 85–95. https://doi.org/10.1016/j.mri.2011.09.003.
[7] Kass, Michael, Andrew Witkin, and Demetri Terzopoulos. 'Snakes: Active Contour Models'. International Journal of Computer Vision 1, no. 4 (January 1988): 321–31. https://doi.org/10.1007/BF00133570.
[8] Chunming Li, Chenyang Xu, Changfeng Gui, and Martin D Fox. 'Distance Regularized Level Set Evolution and Its Application to Image Segmentation'. IEEE Transactions on Image Processing 19, no. 12 (December 2010): 3243–54. https://doi.org/10.1109/TIP.2010.2069690.
[9] Nourmohamadi, Maryam, and Hossein Pourghassem. 'Dermoscopy Image Segmentation Using a Modified Level Set Algorithm'. In 2012 Fourth International Conference on Computational Intelligence and Communication Networks, 286–90. Mathura, Uttar Pradesh, India: IEEE, 2012. https://doi.org/10.1109/CICN.2012.80.
[10] Moreno, Juan C., V.B. Surya Prasath, Hugo Proença, and K. Palaniappan. 'Fast and Globally Convex Multiphase Active Contours for Brain MRI Segmentation'. Computer Vision and Image Understanding 125 (August 2014): 237–50. https://doi.org/10.1016/j.cviu.2014.04.010.
[11] Duth, P. Sudharshan, C. A. Vipuldas, and V. P. Saikrishnan. 'Integrated Spatial Fuzzy Clustering with Variational Level Set Method for MRI Brain Image Segmentation'. In 2017 International Conference on Communication and Signal Processing (ICCSP), 1559–62. Chennai: IEEE, 2017. https://doi.org/10.1109/ICCSP.2017.8286650.
[12] Chunming Li, Rui Huang, Zhaohua Ding, J C Gatenby, D N Metaxas, and J C Gore. 'A Level Set Method for Image Segmentation in the Presence of Intensity Inhomogeneities With Application to MRI'. IEEE Transactions on Image Processing 20, no. 7 (July 2011): 2007–16. https://doi.org/10.1109/TIP.2011.2146190.
[13] Liu, Yu, Gabriella Captur, James C. Moon, Shuxu Guo, Xiaoping Yang, Shaoxiang Zhang, and Chunming Li. 'Distance Regularized Two Level Sets for Segmentation of Left and Right Ventricles from Cine-MRI'. Magnetic Resonance Imaging 34, no. 5 (June 2016): 699–706. https://doi.org/10.1016/j.mri.2015.12.027.
[14] Wali, Samad, Chunming Li, Mudassar Imran, Abdul Shakoor, and Abdul Basit. 'Level-Set Evolution for Medical Image Segmentation with Alternating Direction Method of Multipliers'. Signal Processing 211 (October 2023): 109105. https://doi.org/10.1016/j.sigpro.2023.109105.
[15] Cai, Qing, Huiying Liu, Sanping Zhou, Jingfeng Sun, and Jing Li. 'An Adaptive-Scale Active Contour Model for Inhomogeneous Image Segmentation and Bias Field Estimation'. Pattern Recognition 82 (October 2018): 79–93. https://doi.org/10.1016/j.patcog.2018.05.008.
[16] Weng, Guirong, Bin Dong, and Yu Lei. 'A Level Set Method Based on Additive Bias Correction for Image Segmentation'. Expert Systems with Applications 185 (December 2021): 115633. https://doi.org/10.1016/j.eswa.2021.115633.
[17] Wang, Hui, Ting-Zhu Huang, Zongben Xu, and Yilun Wang. 'An Active Contour Model and Its Algorithms with Local and Global Gaussian Distribution Fitting Energies'. Information Sciences 263 (April 2014): 43–59. https://doi.org/10.1016/j.ins.2013.10.033.
[18] Wang, Hui, Ting-Zhu Huang, Zhi Xu, and Yugang Wang. 'A Two-Stage Image Segmentation via Global and Local Region Active Contours'. Neurocomputing 205 (September 2016): 130–40. https://doi.org/10.1016/j.neucom.2016.03.050.
[19] Wang, Lei, Sheng Wang, Yi Liao, Xiufen Ye, and Tian Wang. 'Improved Level Set Model for Color Image Segmentation'. In 2018 IEEE International Conference on Mechatronics and Automation (ICMA), 574–78. Changchun: IEEE, 2018. https://doi.org/10.1109/ICMA.2018.8484379.
[20] Jing, Xu, Wu Jian, Ye Feng, and Cui Zhi-ming. 'A Level Set Method for Color Image Segmentation Based on Bayesian Classifier'. In 2008 International Conference on Computer Science and Software Engineering, 886–90. Wuhan, China: IEEE, 2008. https://doi.org/10.1109/CSSE.2008.1193.
[21] T. F. Chan and L. A. Vese, "Active contours without edges," in IEEE Transactions on Image Processing,. Feb. 2001 .
[22] C. Li, C. -Y. Kao, J. C. Gore and Z. Ding, "Minimization of Region-Scalable Fitting Energy for Image Segmentation," in IEEE Transactions on Image Processing, Oct. 2008.